



# A universal velocity transformation for boundary layers with pressure gradients

Peng E.S. Chen<sup>1,†</sup>, Wen Wu<sup>2</sup>, Kevin P. Griffin<sup>3,4</sup>, Yipeng Shi<sup>1</sup> and Xiang I.A. Yang<sup>5</sup>

<sup>1</sup>Department of Mechanics and Engineering Science, Peking University, Beijing 100871, PR China

<sup>2</sup>Department of Mechanical Engineering, University of Mississippi, MS 38677, USA

<sup>3</sup>Center for Turbulence Research, Stanford University, CA 94305, USA

<sup>4</sup>National Renewable Energy Laboratory, CO 80401, USA

<sup>5</sup>Mechanical Engineering, Pennsylvania State University, PA 16802, USA

(Received 8 January 2023; revised 14 June 2023; accepted 1 July 2023)

The logarithmic law of the wall does not capture the mean flow when a boundary layer is subjected to a strong pressure gradient. In such a boundary layer, the mean flow is affected by the spatio-temporal history of the imposed pressure gradient; and accounting for history effects remains a challenge. This work aims to develop a universal mean flow scaling for boundary layers subjected to arbitrary adverse or/and favourable pressure gradients. We derive from the Navier–Stokes equation a velocity transformation that accounts for the history effects and maps the mean flow to the canonical law of the wall. The transformation is tested against channel flows with a suddenly imposed adverse or favourable pressure gradient, boundary layer flows subjected to an adverse pressure gradient, and Couette–Poiseuille flows with a streamwise pressure gradient. It is found that the transformed velocity profiles follow closely the equilibrium law of the wall.

**Key words:** turbulent boundary layers, turbulence theory, Navier–Stokes equations

## 1. Introduction

Boundary layers subjected to favourable pressure gradients (FPGs) or adverse pressure gradients (APGs) are common in fluid engineering. In the past 30 years, many have studied boundary layers with pressure gradients, including theory work (Perry, Marusic & Jones 1998; Nickels 2004; Wei, Fife & Klewicki 2007; Wei, Maciel & Klewicki 2017; Subrahmanyam, Cantwell & Alonso 2022), experimental work (Aubertine & Eaton 2005; Harun *et al.* 2013; Volino 2020; Parthasarathy & Saxton-Fox 2022; Romero *et al.* 2022b)

† Email address for correspondence: [chenpeng66@pku.edu.cn](mailto:chenpeng66@pku.edu.cn)

and computational work (Lee & Sung 2009; Inoue *et al.* 2013; Kitsios *et al.* 2017; Lee 2017; Subrahmanyam *et al.* 2023), to name a few of the previous works. It was known that the mean flow responds to pressure gradients faster than the turbulence. It has also been found that there are history effects, and the law of the wall loses its predictive power. However, it is unclear how one can account for history effects in a mean flow scaling. Consequently, no good mean flow scaling exists for boundary layers with pressure gradients. This work aims to account for history effects in the mean flow scaling and establish a universal mean flow scaling for boundary layers subjected to arbitrary APGs and FPGs.

We begin our discussion by estimating the pressure gradients encountered in engineering flows. Consider, for example, the boundary layer on the suction side of an aerofoil, such as sterns on an underwater vehicle or a turbine blade. At large angles of attack, the pressure gradient causes an appreciable change in the fluid velocity. An order-of-magnitude estimate of the pressure gradient is

$$\left| \frac{dP}{ds} \right| = \alpha \frac{\rho U_0^2}{c}, \tag{1.1}$$

where  $dP/ds$  is the pressure gradient along a streamline,  $U_0$  is the velocity of the incoming fluid,  $c$  is the chord length, and  $\alpha$  is an order 0.1 factor. Define

$$\Pi \equiv \frac{\delta}{\rho \tau_w} \left| \frac{dP}{ds} \right|, \tag{1.2}$$

where  $\delta$  is the boundary layer thickness, and  $\tau_w = \nu dU/dy$  is the wall-shear stress. We have

$$\Pi = \frac{\delta}{\rho \tau_w} \frac{\alpha \rho U_0^2}{c} = \frac{2\alpha \delta / c}{C_f}. \tag{1.3}$$

A rough estimate according to Anderson (2011) is

$$C_f \sim O(10^{-4} - 10^{-3}), \quad \alpha \delta / c \sim O(0.001 - 0.01), \tag{1.4a,b}$$

which leads to

$$\Pi \sim O(1) \text{ to } O(100). \tag{1.5}$$

Following this estimate, we limit ourselves to  $|\Pi|$  between 1 and 100. Flows subjected to a pressure gradient with  $\Pi < 1$  will be in a quasi-equilibrium state, and flows subjected to a pressure gradient with  $\Pi > 100$  are rare.

Consider the scaling of the mean velocity. The canonical law of the wall (LoW) provides a good working approximation of the mean flow in a zero pressure gradient (ZPG) boundary layer. Here, the LoW refers to the scaling of the mean flow in the constant stress layer (or the inner layer), where the inner scaled velocity follows a linear and a logarithmic scaling of the inner scaled distance from the wall for  $y \lesssim 5\nu/u_\tau$  and  $\nu/u_\tau \ll y \ll \delta$ , respectively:

$$\left. \begin{aligned} U^+ &= y^+ \quad \text{for } y \lesssim 5\nu/u_\tau, \\ U^+ &= \frac{1}{\kappa} \log(y^+) + B \quad \text{for } \nu/u_\tau \ll y \ll \delta. \end{aligned} \right\} \tag{1.6}$$

The behaviour of the mean flow in the buffer layer is also a function of  $y^+$  only, but there is no accepted explicit expression. Here,  $U^+ = U/u_\tau$ , where  $U$  is the mean velocity,  $u_\tau$  is the friction velocity,  $y^+ = yu_\tau/\nu$ ,  $\nu$  is the kinematic viscosity,  $y$  is the wall-normal coordinate,

*A universal velocity transformation for boundary layers*

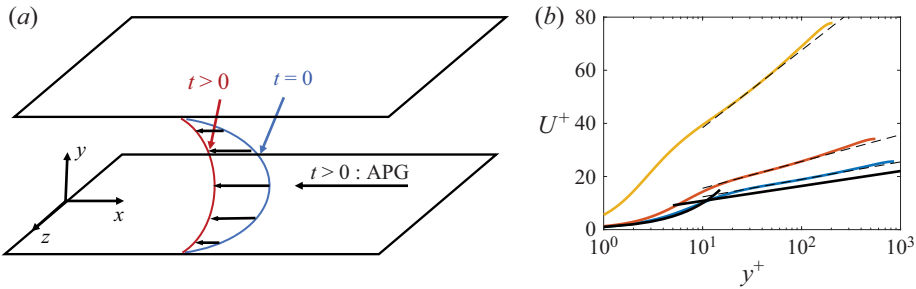


Figure 1. (a) Schematic of the model problem. A fully developed channel is subjected to a suddenly imposed APG and decelerates as a result. (b) Mean velocity profiles at a few time instants. The flow is initially at a Reynolds number  $Re_\tau = 1000$ . An APG  $\Pi = +100$  is imposed at  $t = 0$ . Shown here are velocity profiles at  $tu_{\tau,0}/\delta = 0.005$  (blue),  $0.035$  (red) and  $0.065$  (yellow). The profiles are normalized with the density  $\rho$ , viscosity  $\mu$  and instantaneous wall shear stress  $\tau_w(t)$ . The dashed lines correspond to (1.6), but we allow  $\kappa$  and  $B$  in (1.6) to vary. Best fits yield  $\kappa = 0.35, 0.23, 0.079$  and  $B = 5.8, 5.48, 9.2$  at  $tu_{\tau,0}/\delta = 0.005, 0.035, 0.065$ , respectively.

$\delta$  is an outer length scale (e.g. boundary layer thickness, half-channel height, pipe radius),  $\kappa \approx 0.4$  is the von Kármán constant (keeping only one significant digit), and  $B \approx 5$  is a constant (Kim, Moin & Moser 1987; Monty *et al.* 2009; Smits, McKeon & Marusic 2011; Marusic *et al.* 2013; Morrill-Winter, Philip & Klewicki 2017). Equation (1.6) fails when the boundary layer is subjected to a strong pressure gradient (Spalart & Watmuff 1993; Nagib & Chauhan 2008; Monty, Harun & Marusic 2011). For illustrative purposes, consider the model problem sketched in figure 1(a), where a fully developed channel is subjected to a suddenly imposed APG. Figure 1(b) shows the velocity profiles in inner units, at a few time instants after an APG  $\Pi = 100$  is imposed suddenly on a  $Re_{\tau,0} = u_{\tau,0}\delta/\nu = 1000$  channel. Beside that the velocity is above the log law, the region within which  $U^+ = y^+$  also retreats, which is quite peculiar. We discuss the scaling of the mean flow in the viscous sublayer in Appendix A. Define

$$\Delta p^+ \equiv \frac{\nu}{\rho u_\tau^3} \frac{dP}{dx} \quad \text{and} \quad \beta \equiv \frac{\delta^*}{\rho u_\tau^2} \frac{dP}{dx}, \quad (1.7a,b)$$

which are common non-dimensional measures of the APG, with  $\beta$  being the Clauser pressure gradient coefficient,  $\delta^*$  being the displacement height, and  $\rho$  being the fluid density. The displacement height in a channel flow is defined as

$$\delta^* = \int_0^\delta \left(1 - \frac{U}{U_c}\right) dy, \quad (1.8)$$

where  $\delta$  is the half-channel height, and  $U_c$  is the mean streamwise velocity at the centreline. Here, the Clauser parameter is the ratio of the two quantities that cause the momentum thickness to increase in a spatially developing boundary layer (in the momentum integral equation). We will report both  $\Delta p^+$  (Nickels 2004; Johnstone, Coleman & Spalart 2010; Lozano-Durán *et al.* 2020; Knopp *et al.* 2021) and  $\beta$  in the following for completeness. For this model problem,  $\Delta p^+ = 0.1$ ,  $\beta = 11.6$  at the initial state.

We see clear history effects in figure 1(b): the same force leads to different velocity profiles at different time instances. This is quite expected: since  $F = ma$  and  $Ft = m \Delta V$ , the change in the fluid velocity is determined not solely by the instantaneous force but by

the force acting on the fluid parcel for a period of time. Such history effects were also noted in Perry, Marusic & Jones (2002), Bobke *et al.* (2017), Volino (2020) and Romero *et al.* (2022*b*), among others. We see from figure 1(*b*) that the LoW in (1.6) with  $\kappa = 0.4$  and  $B = 5$  does not fit the data, not even the lower part of the velocity profiles, which is in contrast to Galbraith, Sjolander & Head (1977), Perry (1966) and Spalart & Watmuff (1993). By varying the two ‘constants’ in the log law, (1.6) fits the mean flow in the inner layer (Nagib & Chauhan 2008; Lee & Sung 2009; Knopp *et al.* 2021), as indicated by the black dashed lines in figure 1. Here, the inner layer is the layer where the outer length scale does not play a role. In most studies, this layer is considered as  $y \lesssim 0.15\delta$ . However, tuning  $\kappa$  and  $B$  to fit data reduces the modelling task to a fitting exercise. The same can be said about the half power law (Stratford 1959; Perry & Schofield 1973; Knopp *et al.* 2021) and other laws (Perry 1966; Perry, Bell & Joubert 1966; Ding *et al.* 2019; Subrahmanyam *et al.* 2022) where one must also adjust the ‘constants’ to fit data. Although the LoW also contains constants, i.e.  $\kappa$  and  $B$ , that must be calibrated against data, the fact that one does not need to adjust these two constants as a function of the Reynolds number makes the LoW ‘universal’.

This work aims to establish a universal mean velocity scaling for wall-bounded flows subjected to arbitrary streamwise pressure gradients. Here, universality is with respect to the pressure gradient and its history. Mean flow scalings are usually explicit algebraic relations with the normalized velocity on the left-hand side and the dependent variables on the right-hand side (Volino 2020; Romero *et al.* 2022*a*). If we were to follow this path, we would be looking for a scaling for  $U$  as a function of the inner and outer length scales and the history of the pressure gradients, which is a daunting task. Instead, we will pursue the idea of velocity transformation. This idea has received much attention in the high-Mach-number-flow literature (Huang & Coleman 1994; Trettel & Larsson 2016; Volpiani *et al.* 2020; Griffin, Fu & Moin 2021). The goal of these transformations is to find  $U_m$  and  $L_m$ ,

$$U^* = \int_0^U \frac{1}{U_m} dU, \quad y^* = \int_0^y \frac{1}{L_m} dy, \quad (1.9a,b)$$

such that the transformed velocity  $U^*$  follows the LoW and is a function of  $y^*$  irrespective of the density variation in the flow (Van Driest 1951; Modesti & Pirozzoli 2019; Modesti, Pirozzoli & Grasso 2019). We have a similar goal, but instead of equilibrium boundary layers, we study non-equilibrium boundary layers subjected to streamwise pressure gradients. The objective is to find a transformation such that the transformed velocity  $U^*$  follows the LoW and is a function of  $y^*$  only, irrespective of the pressure gradient.

The rest of the paper is organized as follows. We derive the transformation in § 2. Details of the validation direct numerical simulations (DNS) data are presented in § 3, followed by test results in § 4. Finally, we conclude in § 5.

## 2. Velocity transformation

In this section, we derive the velocity transformation from the Navier–Stokes equation and discuss its properties.

### 2.1. Assumptions

The derivation assumes the following. First, the flow is incompressible. Second, the mean flow is two-dimensional. This holds when the pressure gradients are in the streamwise direction. Third, the boundary layer is thin with respect to its rate of growth. That is, the

## A universal velocity transformation for boundary layers

velocity gradient in the wall-normal direction is much larger than that in the streamwise direction (which is only approximately true for boundary layers but is exactly true for channel flow). This assumption limits the discussion to attached flows, i.e. before incipient separation. Fourth, the flow is assumed to be initially in an equilibrium state. That is, the mean flow initially conforms to the LoW. Fifth, it is assumed that a universal velocity transformation exists. Define

$$f \equiv \frac{dU^*}{dy^*} (1 + v_t^+). \quad (2.1)$$

Here,  $v_t^+ = v_t/\nu$ , where  $\nu$  is the kinematic viscosity,  $v_t = -\langle uv \rangle / (dU/dy)$  is the eddy viscosity, and  $-\langle uv \rangle$  is the Reynolds shear stress. By universality,  $f$  is a function of  $y^*$  only in the inner layer. Like any assumption in any theory, (2.1) facilitates mathematical derivations, and its validity must be verified empirically.

Since the transformed velocity  $U^*$  is a function of the transformed wall-normal coordinate  $y^*$  only, it follows from this universality assumption that  $v_t^+$  is also a function of only  $y^*$  only in the inner layer. In addition, because  $f = 1$  in the inner layer of ZPG boundary layer flows (due to the constant stress layer), the universality assumption implies that  $f \equiv 1$  in all flows – in the layer where the outer length scale does not play a role. Note that we do not need to assume a constant stress layer. The function  $f$ , in general, is a function of  $y/\delta$ .

### 2.2. Governing equation

The Reynolds-averaged streamwise momentum equation reads

$$\frac{\partial U}{\partial t} + U \frac{\partial U}{\partial x} + V \frac{\partial U}{\partial y} = -\frac{1}{\rho} \frac{\partial P}{\partial x} + \frac{\partial \tau_{xx}}{\partial x} + \frac{\partial \tau_{xy}}{\partial y}, \quad (2.2)$$

where

$$\tau_{xx} = 2\nu \frac{\partial U}{\partial x} - \langle u'u' \rangle, \quad \tau_{xy} = \nu \left( \frac{\partial U}{\partial y} + \frac{\partial V}{\partial x} \right) - \langle u'v' \rangle. \quad (2.3a,b)$$

The equation assumes incompressibility and two-dimensional mean flow. Hence the  $\partial/\partial z$  terms are dropped. Here, the uppercase letters denote mean quantities, the lowercase letters denote instantaneous quantities, ' denotes fluctuations,  $x$ ,  $y$  and  $z$  are the streamwise, wall-normal and spanwise directions,  $U$ ,  $V$ ,  $W$  or  $u$ ,  $v$ ,  $w$  give the velocity in the three Cartesian directions,  $\tau$  is the stress, and  $\langle \cdot \rangle$  denotes ensemble averaging. Invoking the thin boundary layer assumption leads to

$$\frac{\partial V}{\partial x} \ll \frac{\partial U}{\partial y}, \quad \frac{\partial \tau_{xx}}{\partial x} \ll \frac{\partial \tau_{xy}}{\partial y}. \quad (2.4a,b)$$

It follows from (2.2), (2.3a,b) and (2.4a,b) that

$$\frac{\partial U}{\partial t} + U \frac{\partial U}{\partial x} + V \frac{\partial U}{\partial y} = -\frac{1}{\rho} \frac{\partial P}{\partial x} + \frac{\partial \tau_{xy}}{\partial y}, \quad (2.5)$$

where

$$\tau_{xy} = \nu \frac{\partial U}{\partial y} - \langle u'v' \rangle. \quad (2.6)$$

We take the  $y$  derivative of both sides of (2.5):

$$\left(\frac{\partial}{\partial t} + U \frac{\partial}{\partial x} + V \frac{\partial}{\partial y}\right) \frac{\partial U}{\partial y} + \frac{\partial U}{\partial y} \frac{\partial U}{\partial x} + \frac{\partial V}{\partial y} \frac{\partial U}{\partial y} = -\frac{1}{\rho} \frac{\partial^2 P}{\partial x \partial y} + \frac{\partial^2 \tau_{xy}}{\partial y^2}. \quad (2.7)$$

We seek to simplify (2.7). First, incompressibility requires

$$\frac{\partial U}{\partial x} + \frac{\partial V}{\partial y} = 0. \quad (2.8)$$

Second, the  $y$  momentum equation reads:

$$\frac{1}{\rho} \frac{\partial P}{\partial y} + \frac{\partial \langle v^2 \rangle}{\partial y} = 0. \quad (2.9)$$

By applying  $\partial/\partial x$  on both sides of (2.9), we have

$$\frac{1}{\rho} \frac{\partial^2 P}{\partial x \partial y} = \frac{\partial^2 \langle v^2 \rangle}{\partial x \partial y} \ll \frac{\partial^2 \tau_{xy}}{\partial y^2}, \quad (2.10)$$

due to the thin boundary layer assumption. Substituting (2.8) and (2.10) into (2.7) leads to

$$\frac{D}{Dt} \frac{\partial U}{\partial y} = \frac{\partial^2 \tau_{xy}}{\partial y^2}. \quad (2.11)$$

Invoking the eddy viscosity  $\nu_t$ , the shear stress term is

$$\tau_{xy} = \nu \frac{\partial U}{\partial y} (1 + \nu_t^+). \quad (2.12)$$

Here,  $\nu_t$  is unspecified. Hence invoking  $\nu_t$  introduces no modelling error. Plugging (1.9a,b) and (2.1) into (2.12), we have

$$\frac{\nu}{\tau_{xy}} \frac{U_m}{L_m} f = 1. \quad (2.13)$$

### 2.3. Transformation

Equations (1.9a,b) and (2.13) lead to

$$U^* = \int_0^U \frac{\nu f}{\tau_{xy}} \frac{dy^*}{dy} dU. \quad (2.14)$$

Equation (2.14) is a velocity transformation, but it requires knowledge of  $y^*$ . In the following, we derive a transformation that maps  $y^+$  to  $y^*$ .

Integrating (2.11) in time, we have

$$\frac{\partial U}{\partial y} = \left(\frac{\partial U}{\partial y}\right)_0 + \int_0^t \frac{\partial^2 \tau_{xy}}{\partial y^2} Dt, \quad (2.15)$$

where the subscript 0 denotes quantities evaluated at the initial state. Note that the integration is Lagrangian. Invoking the assumed initial state, the mean flow abides by

the LoW, therefore,

$$\left(\frac{\partial U}{\partial y}\right)_0 = \left(\frac{u_{\tau}^2}{\nu} \frac{1}{F(y^+)}\right)_0 = \frac{u_{\tau,0}^2}{\nu} \frac{1}{F(y_0^+)}, \quad (2.16)$$

where

$$F(y_0^+) = 1 + \kappa y_0^+ (1 - \exp(-y_0^+/A))^2 \quad (2.17)$$

is a damping function (Van Driest 1956; Kawai & Larsson 2012; Yang & Lv 2018),  $A = 17$  is a constant,  $y_0^+ = \nu u_{\tau,0}/\nu$ , and  $u_{\tau,0}$  is the friction velocity at the initial state. The use of the van Driest damping function is to give the equilibrium  $\partial U/\partial y$  a closed expression. The derivation itself does not necessarily need such an approximation. An alternative definition for  $F$  is

$$F(y_0^+) = \frac{u_{\tau,0}^2}{\nu} \frac{1}{(\partial U/\partial y)_0}, \quad (2.18)$$

where we have left  $(\partial U/\partial y)_0$  as is. Invoking (2.13) and the assumption that  $U^*$  follows the LoW, the left-hand side of (2.15) is

$$\frac{\partial U}{\partial y} = \frac{\tau_{xy}}{\nu f} \frac{1}{F(y^*)}. \quad (2.19)$$

Substituting (2.19) into (2.15) and rearranging, we have

$$F(y^*) = \frac{1}{\left(\frac{\partial U}{\partial y}\right)_0 + \int_0^t \frac{\partial^2 \tau_{xy}}{\partial y^2} Dt} \frac{\tau_{xy}}{\nu f}. \quad (2.20)$$

Here,  $F$  is given in (2.17),  $f \equiv 1$  for  $y \ll \delta$ , its value in the outer layer can be measured at the initial state (as a function of  $y/\delta$ ), and the derivative  $(\partial U/\partial y)_0$  is known from the equilibrium LoW. Equations (2.20) and (2.14) are the transformations that we are looking for.

#### 2.4. Further simplification

We rearrange (2.20) and (2.14) to put them into the standard form as defined in (1.9a,b). First, we define

$$g \equiv \frac{\partial U/\partial y - (\partial U/\partial y)_0}{(\partial U/\partial y)_0}. \quad (2.21)$$

It follows from (2.15), (2.16) and (2.21) that

$$g = \frac{\nu F(y_0^+)}{u_{\tau,0}^2} \int_0^t \frac{\partial^2 \tau_{xy}}{\partial y^2} Dt. \quad (2.22)$$

Equations (2.22) and (2.20) together give

$$y^* = F^{-1} \left[ \frac{1 + g_w}{1 + g} \frac{\tau^+}{f} F(y_0^+) \right]. \quad (2.23)$$

Here,  $F^{-1}$  denotes the inverse function of  $F$ ,  $\tau^+ = \tau_{xy}/\tau_{xy,w}$ , and  $g_w$  is  $g$  evaluated at the wall. Notice that  $\tau^+$  is ill-defined at separation, therefore our scaling is valid up to



incipient separation. The term  $(1 + g_w)/(1 + g)$  in (2.23) accounts for the history effects. Equation (2.23) gives

$$y^* = \int_0^y \frac{F(y^*)}{F'(y^*)} \left[ \frac{f}{\tau^+} \frac{\partial}{\partial y} \left( \frac{\tau^+}{f} \right) - \frac{1}{1 + g} \frac{\partial g}{\partial y} + \frac{F'(y_0^+)}{F(y_0^+)} \frac{dy_0^+}{dy} \right] dy. \tag{2.24}$$

Equations (2.24) and (2.14) give

$$U^* = \int_0^U \frac{vf}{\tau_{xy}} \frac{F(y^*)}{F'(y^*)} \left[ \frac{f}{\tau^+} \frac{\partial}{\partial y} \left( \frac{\tau^+}{f} \right) - \frac{1}{1 + g} \frac{\partial g}{\partial y} + \frac{F'(y_0^+)}{F(y_0^+)} \frac{dy_0^+}{dy} \right] dU. \tag{2.25}$$

Equations (2.24) and (2.25) are the velocity transformation.

### 2.5. Discussion

The transformations are collected below:

$$\left. \begin{aligned} y^* &= \int_0^y \frac{F(y^*)}{F'(y^*)} \left[ \frac{f}{\tau^+} \frac{\partial}{\partial y} \left( \frac{\tau^+}{f} \right) - \frac{1}{1 + g} \frac{\partial g}{\partial y} + \frac{F'(y_0^+)}{F(y_0^+)} \frac{dy_0^+}{dy} \right] dy, \\ U^* &= \int_0^U \frac{vf}{\tau_{xy}} \frac{F(y^*)}{F'(y^*)} \left[ \frac{f}{\tau^+} \frac{\partial}{\partial y} \left( \frac{\tau^+}{f} \right) - \frac{1}{1 + g} \frac{\partial g}{\partial y} + \frac{F'(y_0^+)}{F(y_0^+)} \frac{dy_0^+}{dy} \right] dU. \end{aligned} \right\} \tag{2.26}$$

We have the following remarks. First, the transformation accounts for history effects through the time integral  $g$ . It is interesting to note that the integral is not weighted, therefore the flow does not ‘forget’. In other words, an event at  $t = 0$  and an event at a later time instant contribute equally to the transformation. Second, the transformation is valid in the outer layer as well. The function  $f$  is 1 in the inner layer and varies as a function of  $y/\delta$  outside. By measuring  $f$  from the initial condition as a function of  $y/\delta$ , the transformation should collapse all velocity profiles. Hence the transformation avoids the constant stress layer assumption, at least formally. Third, the transformation is presented as a descriptive tool for now. The transformation shows how history should be accounted for in mean flow scalings. It shows that pressure gradients do not affect the mean flow directly. Instead, they affect the shear stress  $\tau_{xy}$ , which then affects the mean flow. Closures for  $\tau_{xy}$  and  $v_t^+$  are needed for the transformation, a topic that we do not discuss here. Fourth, the transformation involves a function inverse and therefore is not explicit.

In the following, we simplify and rewrite the transformation for the log layer in a ZPG boundary layer, for Couette–Poiseuille flow, for a channel with a suddenly imposed streamwise pressure gradient, and for spatially developing boundary layers with streamwise pressure gradients.

First, for the log and the viscous layers, we have

$$\tau_{xy} = \text{const.} \tag{2.27}$$

It follows that  $g = 0$  and  $\tau^+/f = 1$ . Hence for flows in the constant stress layer, the velocity transformation reduces to  $U^* = U^+$  and  $y^* = y^+$ .

Second, we consider the Couette–Poiseuille flow. Figure 2(a) shows a schematic of the flow. The flow is subjected to an APG near one wall and an FPG near the other. The stress



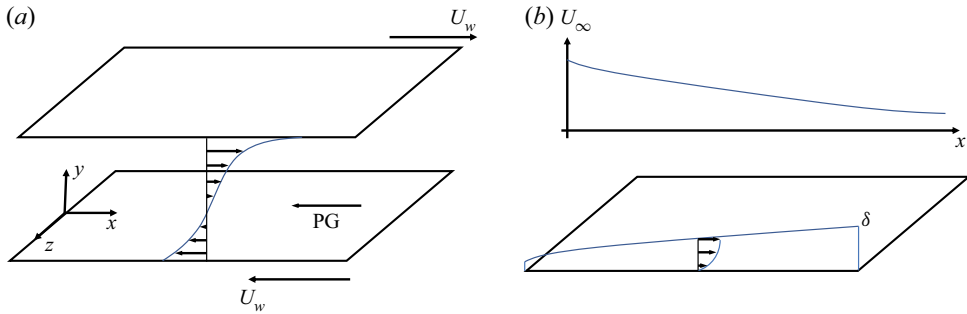


Figure 2. (a) A sketch of Couette–Poiseuille flow. The flow is subjected to an FPG near the top plate and an APG near the bottom plate (Johnstone *et al.* 2010; Coleman & Spalart 2015). (b) A sketch of a boundary layer subjected to APGs. The pressure gradient (PG) is imposed by varying the freestream velocity. The reader is directed to Bobke *et al.* (2017) for more details.

$\tau_{xy}$  is a linear function of  $y$ . The function  $f$  can be measured from the Couette flow, and  $f = 1$ . It follows that  $g = 0$ , therefore (2.23) becomes

$$F(y^*) = \tau^+ F(y^+). \quad (2.28)$$

The velocity transformation becomes

$$U^* = \int_0^U \frac{vf}{\tau_{xy}} \frac{F(y^*)}{F'(y^*)} \left( \frac{1}{\tau^+} \frac{\partial \tau^+}{\partial y} + \frac{F'(y^+)}{F(y^+)} \frac{dy^+}{dy} \right) dU. \quad (2.29)$$

Third, for channel flow with a suddenly imposed streamwise pressure gradient, the mean advection is 0, therefore the Lagrangian integration degenerates to an Eulerian one, i.e.  $Dt = dt$ . It follows that (2.22) becomes

$$g = \frac{\nu F(y_0^+)}{u_{\tau,0}^2} \int_0^t \frac{\partial^2 \tau_{xy}}{\partial y^2} dt, \quad y > 0. \quad (2.30)$$

Furthermore, measuring  $f$  from the initial condition, we have  $f = 1 - y/\delta$ .

Fourth, for a spatially developing turbulent boundary layer with streamwise pressure gradients, Lagrangian integration is along the streamline, and (2.22) becomes

$$g = \frac{\nu F(y_0^+)}{u_{\tau,0}^2} \int_0^t \frac{\partial^2 \tau_{xy}}{\partial y^2} \frac{ds}{|U|}, \quad y > 0, \quad (2.31)$$

where  $ds$  is along a streamline, and  $|U|$  is the velocity magnitude. Equation (2.31) is singular at the wall because of the no-slip condition. However, this singularity is removable. We know that the velocity follows  $U^+ = y^+$  sufficiently close to the wall, irrespective of any non-equilibrium effects. Since  $U^*$  is a universal function of  $y^*$ , we must have  $U^* = y^*$  sufficiently close to the wall as well. This gives directly  $y^* = y^+$  at the wall, thereby removing the singularity at the wall.

### 3. Computational set-up

To test the velocity transformation, we conduct DNS of channel flows subjected to a suddenly imposed APG or FPG. The flow is sketched in figure 1(a). It is a fully developed

Case	$Re_{\tau,0}$	$\Pi_0$	$\beta$	$\Delta p^+ \times 10^3$	$L_x \times L_y \times L_z$	$n_x \times n_y \times n_z$	$\Delta x^+ \times \Delta y^+ \times \Delta z^+$	$N$
R5A1	544	1	[0.13, 3.88]	[1.84, 187]	$4\pi \times 2 \times 2\pi$	$576 \times 243 \times 540$	$11.8 \times (0.048, 7.23) \times 6.32$	3
R5A10	544	10	[1.31, 20.1]	[18.4, 488]	$4\pi \times 2 \times 2\pi$	$576 \times 243 \times 540$	$11.8 \times (0.048, 7.23) \times 6.32$	4
R5A100	544	100	[19.9, 49.5]	[184, 1245]	$4\pi \times 2 \times 2\pi$	$576 \times 243 \times 540$	$11.8 \times (0.048, 7.23) \times 6.32$	12
R5F10	544	-10	[-2.49, -0.94]	[-11.9, -7.6]	$4\pi \times 2 \times 2\pi$	$1024 \times 512 \times 1024$	$13.4 \times (0.13, 6.72) \times 6.70$	1
R5F100	544	-100	[-24.9, -1.93]	[-119, -16.1]	$4\pi \times 2 \times 2\pi$	$1024 \times 512 \times 1024$	$12.6 \times (0.12, 6.32) \times 6.29$	1
R10A10	1000	10	[1.17, 8.17]	[10.1, 91.9]	$8\pi \times 2 \times 3\pi$	$2048 \times 512 \times 1536$	$12.3 \times (0.12, 6.15) \times 6.13$	2
R10A100	1000	100	[11.6, 44.1]	[100, 573]	$8\pi \times 2 \times 3\pi$	$2048 \times 512 \times 1536$	$12.3 \times (0.12, 6.15) \times 6.13$	3

Table 1. DNS details of channel flows subjected to a suddenly imposed adverse ( $\Pi > 0$ ) or favourable ( $\Pi < 0$ ) pressure gradient. Here,  $Re_{\tau,0}$  is the initial Reynolds number;  $\Pi$  is positive for APG and negative for FPG;  $L_x$ ,  $L_y$  and  $L_z$  are the domain sizes in the streamwise, wall-normal and spanwise directions. Normalization is by the half-channel height. Also,  $n_x$ ,  $n_y$  and  $n_z$  are the numbers of grid points in the three Cartesian directions, and  $\Delta x^+$ ,  $\Delta y^+$  and  $\Delta z^+$  are the grid spacings in the three directions. For  $\Delta y^+$ , we list the resolution at the wall and the channel centre. We list the grid resolution at the beginning or the end of the DNS. For  $\Pi > 0$ , a finer grid must be employed at the beginning than at the end, and we list the grid resolution at the beginning of the DNS, and *vice versa*. Parameter  $N$  is the number of ensembles used to compute the flow statistics.

Case	Flow type	Reference	$Re_\tau$	$\Pi$	$\beta$	$\Delta p^+ \times 10^3$
CGSR5A	CP	Coleman <i>et al.</i> (2015)	589	+1.59	—	2.7
CGSR12F	CP	Coleman <i>et al.</i> (2015)	1210	−0.39	—	−0.32
JCSR3A	CP	Johnstone <i>et al.</i> (2010)	336	+1.24	—	3.7
JCSR6F	CP	Johnstone <i>et al.</i> (2010)	627	−0.36	—	−0.57
m13	APG-BL	Bobke <i>et al.</i> (2017)	[190, 896]	[3.80, 5.51]	[0.86, 1.49]	[5.0, 21.3]
m16	APG-BL	Bobke <i>et al.</i> (2017)	[189, 934]	[5.82, 8.67]	[1.55, 2.55]	[10.9, 27.7]
m18	APG-BL	Bobke <i>et al.</i> (2017)	[192, 973]	[7.29, 12.5]	[2.15, 4.07]	[16.0, 33.6]
b1	APG-BL	Bobke <i>et al.</i> (2017)	[190, 862]	$\approx 4.11$	$\approx 1$	[5.1, 14.3]
b2	APG-BL	Bobke <i>et al.</i> (2017)	[189, 910]	$\approx 7.55$	$\approx 2$	[10.6, 20.8]
ZPG	ZPG-BL	Schlatter & Örlü (2010)	[252; 1271]	0	0	0

Table 2. Details of the Couette–Poiseuille (CP) flows and the boundary layer (BL) flows. The nomenclature is [Initial of authors][ $Re_\tau/100$ ][PG], where  $Re_\tau$  is the friction Reynolds number. Further details of the flows can be found in Coleman, Garbaruk & Spalart (2015) and Johnstone *et al.* (2010), and are not repeated here for brevity. The velocity in a Couette–Poiseuille flow increases monotonically from one wall to the other. It is therefore not straightforward to define the heights of the boundary layers near the two walls. Consequently, defining  $\beta$  is not straightforward for Couette–Poiseuille flow. The nomenclature of the BL cases is the same as in Bobke *et al.* (2017). The ranges of  $Re_\tau$  and  $\Pi$  are shown in the table. Note that for cases b1 and b2,  $\Pi$  is approximately a constant, while for cases m13, m16 and m18, it is varying. We also include the ZPG-BL data in Schlatter & Örlü (2010) for comparison purposes.

two-dimensional turbulent channel. At  $t = 0$ , a constant pressure gradient  $dP/dx$  is imposed suddenly, and subsequently held constant for the duration of the simulation. The mean flow evolves with time as a result.

Table 1 shows the DNS details. The nomenclature is as follows:  $R[Re_{\tau,0}/100]F/A[|\Pi|]$ , where  $F$  is for FPG, and  $A$  is for APG. For APGs,  $\Pi$  is 1, 10 or 100, corresponding to a weak APG, a moderate APG, and a strong APG. For FPGs,  $\Pi = -10$  or  $-100$ , corresponding to a moderate or strong FPG. FPGs are not very challenging (or interesting) because the canonical LoW works reasonably well for flows with FPGs (Townsend 1956; Mellor & Gibson 1966), although FPGs have interesting effects on the eddies in the flow (Volino 2020). The initial Reynolds number is  $Re_{\tau,0} = 544$  or 1000. The Reynolds number increases when an FPG is applied and decreases when an APG is applied. The size of the channel is  $(4\pi \times 2 \times 2\pi)\delta$  for the R5 ( $Re_{\tau,0} = 544$ ) cases, and  $(8\pi \times 2 \times 3\pi)\delta$  for the R10 ( $Re_{\tau,0} = 1000$ ) cases. The domain sizes for the R5 and R10 cases are different because the initial fields were generated by different authors. Nonetheless, both domains are larger than that of the minimal channel (Lozano-Durán & Jiménez 2014). The grid resolution is comparable to that in Mathur *et al.* (2018) and Yang *et al.* (2021), and is such that the flow is well-resolved from the beginning to the end. We employ statistically uncorrelated initial flow fields, and repeat the simulations multiple times to get converged statistics following Lozano-Durán *et al.* (2020), Chung (2005) and He & Seddighi (2015). The code that we use is the same as in Lee & Moser (2015). Details of the code can be found in Graham *et al.* (2016) and Lee & Moser (2015), and are not detailed here for brevity.

We will also use the boundary layer data in Bobke *et al.* (2017), and the Couette–Poiseuille data in Coleman & Spalart (2015) and Johnstone *et al.* (2010). The flows are sketched in figure 2. Flow parameters that are relevant to this analysis are tabulated in table 2. Further details are not shown here for brevity.

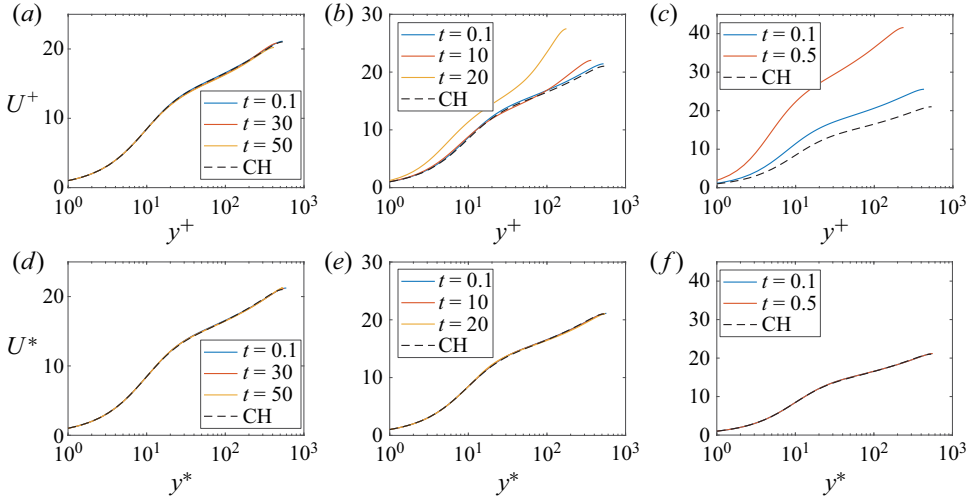


Figure 3. Mean velocity profiles at a few time instants. (a–c) Plots of  $U^+$  as a function of  $y^+$ . Here, normalization is by the wall-shear stress at time  $t$ . (d–f) Plots of  $U^*$  as a function of  $y^*$ . Here,  $U^*(y^*)$  is the transformed velocity. Cases: (a,d) R5A1, (b,e) R5A10, (c,f) R5A100. Here, time  $t$  is normalized with  $\delta/u_{\tau,0}$ . CH is the velocity profile in a fully developed  $Re_{\tau} = 544$  channel.

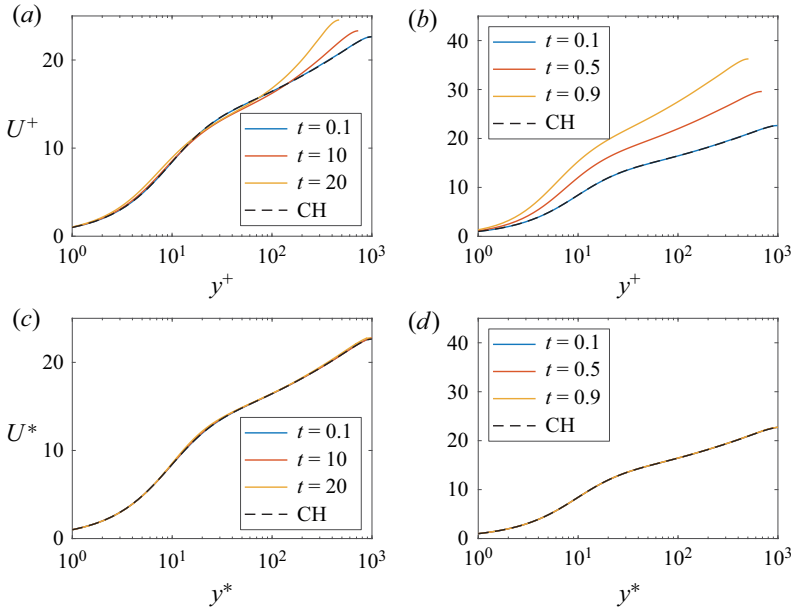


Figure 4. Mean velocity profiles at a few time instants. (a,b) Plots of  $U^+$  as a function of  $y^+$ . Here, normalization is by the wall-shear stress at time  $t$ . (c,d) Plots of  $U^*$  as a function of  $y^*$ . Here,  $U^*(y^*)$  is the transformed velocity. Cases: (a,c) R10A10, (b,d) R10A100. CH is the velocity profile in a fully developed  $Re_{\tau} = 1000$  channel.

## 4. Results

### 4.1. Channel flow results

First, we present the channel flow results. Figures 3 and 4 show the mean velocity profiles in the APG cases. Figure 3 shows the R5 results, and figure 4 shows the R10 results.

A universal velocity transformation for boundary layers

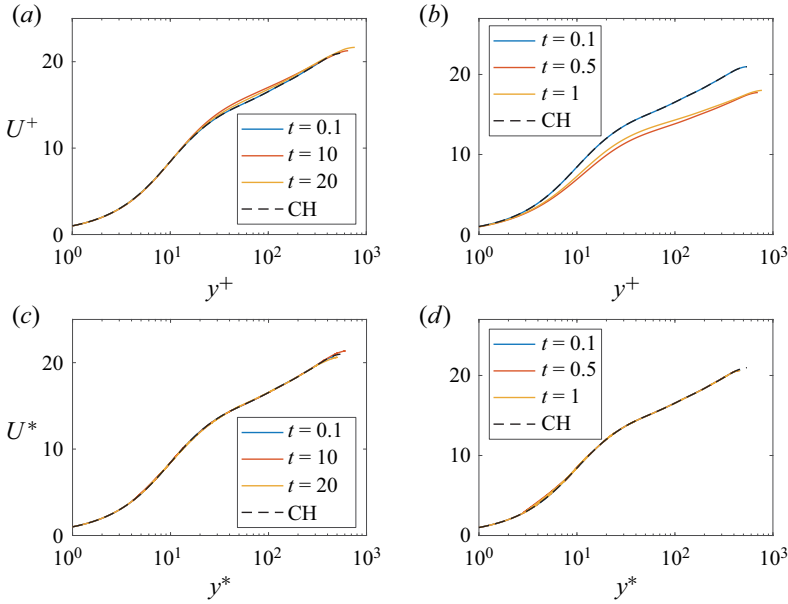


Figure 5. Mean velocity profiles at a few time instants. (a,b) Plots of  $U^+$  as a function of  $y^+$ . Here, normalization is by the wall-shear stress at time  $t$ . (c,d) Plots of  $U^*$  as a function of  $y^*$ . Here,  $U^*(y^*)$  is the transformed velocity. Cases: (a,c) R5F10, (b,d) R5F100. CH is the velocity profile in a fully developed  $Re_\tau = 544$  channel.

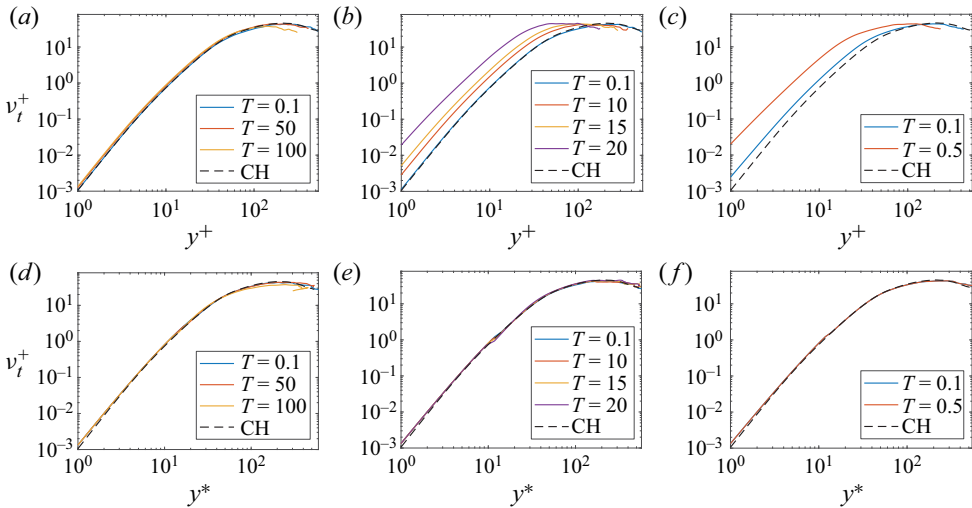


Figure 6. Eddy viscosity at various time instants. (a–c) Plots of  $v_t^+$  as a function of  $y^+$ . (d–f) Plots of  $v_t^+$  as a function of  $y^*$ . Cases: (a,d) R5A1, (b,e) R5A10, (c,f) R5A100.

The results at other time instants are similar and are not shown here for brevity. In R5A1, a weak APG is applied, and the flow is at a quasi-equilibrium state. As a result, both  $U^+$  and  $U^*$  follow the LoW. In R5A10 and R10A10, a moderate APG is applied, and we see noticeable deviations in  $U^+$  from the LoW after the APG has acted on the flow for some time at  $t = O(10)$ . On the other hand, the transformed velocity  $U^*$  follows the LoW closely

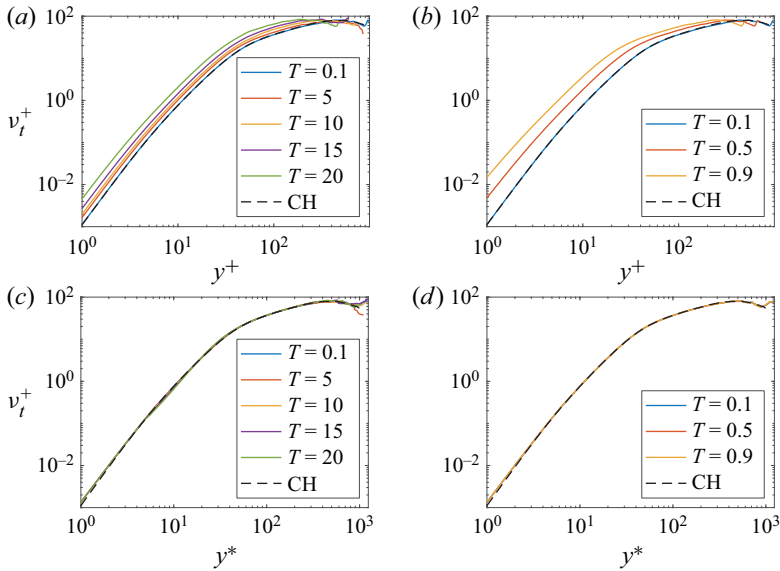


Figure 7. Same as figure 6 but for the R10 cases: (a,c) R10A10, (b,d) R10A100.

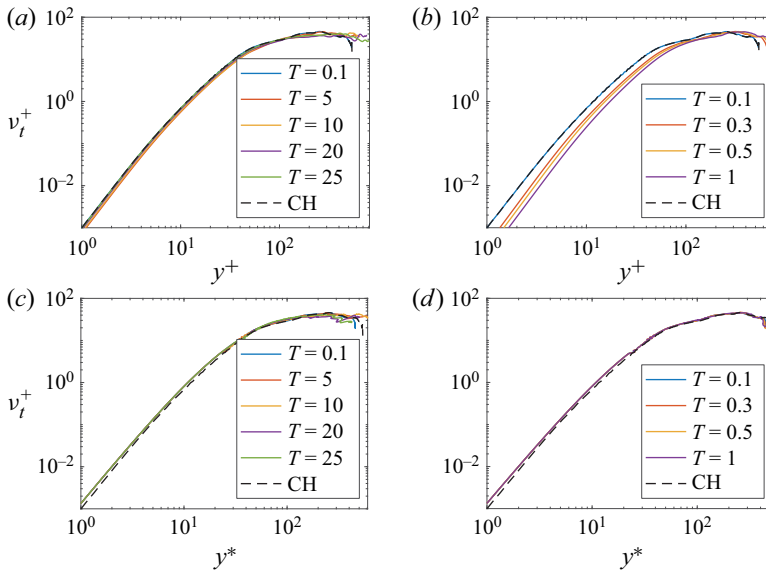


Figure 8. Same as figure 6 but for the R5F cases: (a,c) R5F10, (b,d) R5F100.

at all time instants. In R5A100 and R10A100, a strong APG is applied. The viscous units fail to collapse the velocity profiles, and only  $U^*$  follows the LoW.

Figure 5 shows the mean velocity profiles in the two FPG cases. FPGs give rise to noticeable deviations from the LoW in R5F100 when the velocity and the wall-normal coordinate are normalized using the viscous units. Nonetheless, the transformed velocity profiles collapse and follow the LoW.

Per the universality assumption, the viscous scaled eddy viscosity is a universal function of the transformed wall-normal coordinate  $y^*$ . In § 2, we noted: ‘Like any assumption in any theory, (2.1) facilitates mathematical derivations, and its validity must be verified

## A universal velocity transformation for boundary layers

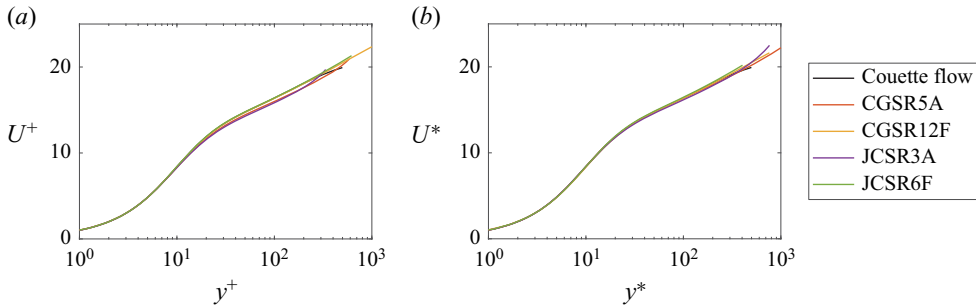


Figure 9. Mean velocity profiles in Couette–Poiseuille flows (a) before and (b) after the transformation.

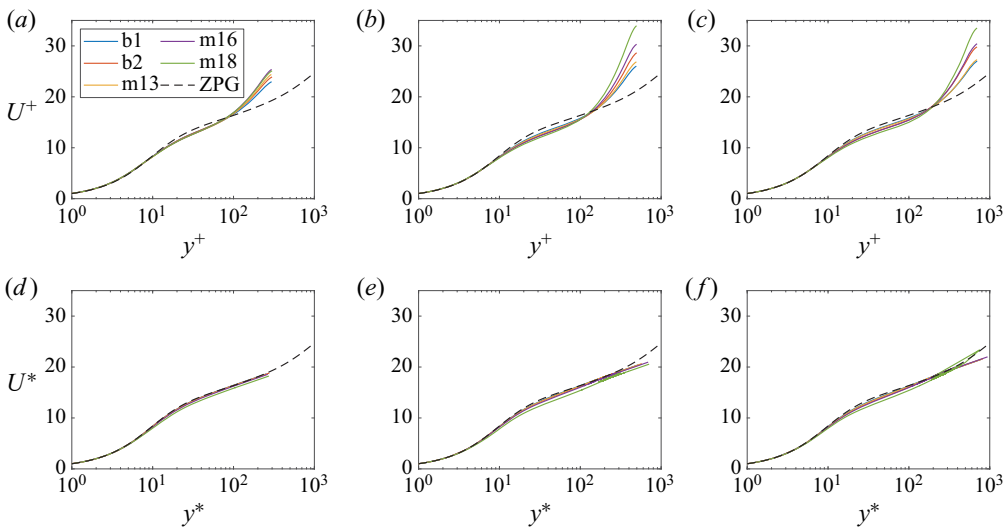


Figure 10. Mean velocity profiles in boundary layer flows at multiple streamwise locations: (a,d)  $Re_\tau = 300$ , (b,e)  $Re_\tau = 500$ , (c,f)  $Re_\tau = 700$ . ZPG is the velocity profile in a zero pressure gradient boundary layer at  $Re_\tau = 1272$ .

empirically.’ In the following, we test (2.1) against empirical data. Figures 6 and 7 show the eddy viscosity in the APG cases. Figure 6 shows the R5 results, and figure 7 shows the R10 results. The flow in R5A1 is at a quasi-equilibrium state,  $y^+$  and  $y^*$  are not very different, and  $v_i^+$  collapses well when plotted as a function of both  $y^+$  and  $y^*$ . In R5A10, R5A100, R10A10 and R10A100, the pressure gradients are strong, the conventional viscous scaling does not collapse data, and only the transformed wall-normal coordinate collapses data. Figure 8 shows the normalized eddy viscosity of the FPG cases. The results are similar to the APG cases: the viscous scaling does not collapse data, whereas the transformed coordinate does. These results verify the universality assumption.

### 4.2. Couette–Poiseuille and boundary layer flows

Next, we show the Couette–Poiseuille flow results. Figure 9 shows the mean velocity profiles before and after the transformation. The flows are subjected to fairly weak pressure



gradients. As a result, the viscous scaled velocity profiles do not deviate far from the LoW, and the velocity transformation leads to a slightly better collapse of the velocity profiles.

Finally, [figure 10](#) shows the boundary layer results. The transformation collapses all profiles, and the transformed velocity profiles follow the LoW. However, the collapse is less convincing compared to the results in [figures 3](#) and [4](#). We think that this is a lack of statistical convergence – compared to channel flow, where one can average among many ensembles and in the two homogeneous directions, the boundary layer is amenable to averaging in time and the spanwise direction. A lack of statistical convergence incurs errors in the derivative calculations, which in turn affect the quality of the data collapse – an aspect that needs further attention.

## 5. Conclusions

We derived a velocity transformation that maps the mean velocity profiles in boundary layers with pressure gradients to the canonical law of the wall (LoW) before incipient separation. The Navier–Stokes equation alone does not give the transformation. Like the semi-local transformation that relies on the assumption that  $v_t^+$  is a universal function of  $y_{st}^*$ , our transformation relies on [\(2.1\)](#), a direct consequence of which is that  $v_t^+$  is a universal function of  $y^*$ . In addition to [\(2.1\)](#), we assume two-dimensional attached mean flows at low speeds, and the knowledge of the mean flow at the equilibrium condition.

The derived transformation contains mean flow information and shear stress information only. History effects are accounted for via a Lagrangian integral of the total shear stress originating from the initial equilibrium state. The transformation suggests that it is the total shear stress that plays into the hysteresis in the mean flow. Furthermore, since the integration weights all historical events equally, the flow does not forget unless the effects of one event are cancelled by another.

The validity of the transformation is tested in channel flows subjected to suddenly imposed pressure gradients, Couette–Poiseuille flows, and spatially developing turbulent boundary layers with moderate APGs. We show that while the inner-unit scaled velocity profiles deviate from the LoW, the transformed profiles follow the LoW closely, irrespective of the streamwise pressure gradients. Further validation of the scaling will be pursued in future studies.

Finally, we comment on the practicality of the present transformation. The LoW is the cornerstone of many wall-bounded turbulence models. However, since the LoW is valid for equilibrium boundary layers only, the reliance on the LoW is a major source of uncertainty in turbulence modelling. As a result, there has always been a need for universal mean flow scalings for non-equilibrium boundary layers. This work will help to address that need. While this paper presented the velocity transformation as a descriptive tool, future work will explore its potential for predictive modelling. Consider, for example, RANS modelling. At a given iteration, one would have a velocity field, which allows one to compute the eddy viscosity and the total shear stress to get to the next iteration. When computing the eddy viscosity in the wall layer, one often needs a damping function. The available damping functions are functions of  $y^+$  (or constructed assuming they are functions of  $y^+$ ), which is based on the LoW and therefore is not always accurate. Our scaling can be used to augment the damping function. The resulting damping function would depend on the Lagrangian history of the total shear stress, but the information is solved for and is available in the simulation. We will leave such practical applications to future studies.

**Acknowledgements.** This work was authored in part by the National Renewable Energy Laboratory, operated by Alliance for Sustainable Energy, LLC, for the US Department of Energy (DOE) under contract no. DE-AC36-08GO28308. The views expressed in the paper do not necessarily represent the views of the DOE or the US Government. The publisher, by accepting the paper for publication, acknowledges that the US Government retains a non-exclusive, paid-up, irrevocable, worldwide licence to publish or reproduce the published form of this work, or allow others to do so, for US Government purposes.

**Funding.** P.E.C. and Y.S. acknowledge financial support from NSFC 91752202. X.I.Y. acknowledges the 2022 CTR summer program and Office of Naval Research, contract no. N000142012315 for financial support. W.W. acknowledges support from NSF grant no. 2131942 for visiting CTR in the summer of 2022. X.I.Y. thanks P. Moin, A. Elnahas, R. Agrawal, A. Lozano-Duran, J. Bae, O. Marxen, M. Cui and M. Momen for their generous help during his stay at Stanford, and he thanks J. Larsson, G. Huang, S. Pirozzoli and I. Marusic for comments. K.P.G. is supported by the Exascale Computing Project (grant 17-SC-20-SC), a collaborative effort of two US Department of Energy organizations (Office of Science and the National Nuclear Security Administration) responsible for the planning and preparation of a capable exascale ecosystem, including software, applications, hardware, advanced system engineering and early testbed platforms, in support of the nation's exascale computing imperative.

**Declaration of interests.** The authors report no conflict of interest.

**Author ORCIDs.**

-  Peng E.S. Chen <https://orcid.org/0000-0001-6387-4811>;
-  Wen Wu <https://orcid.org/0000-0003-4241-1716>;
-  Kevin P. Griffin <https://orcid.org/0000-0002-0866-6224>;
-  Xiang I.A. Yang <https://orcid.org/0000-0003-4940-5976>.

**Appendix A. Mean flow scaling in the viscous sublayer**

We discuss the scaling of the mean flow in the viscous sublayer.

First, expanding the mean velocity according to Taylor series in the wall layer gives

$$U = \frac{\partial U}{\partial y} \Big|_w y + \frac{1}{2} \frac{\partial^2 U}{\partial y^2} \Big|_w y^2 + O(y^3). \tag{A1}$$

The definition of  $\tau_w$  gives

$$\frac{\partial U}{\partial y} \Big|_w = \frac{\tau_w(t)}{\nu}. \tag{A2}$$

Evaluating the Navier–Stokes equation at the wall gives

$$\frac{\partial^2 U}{\partial y^2} \Big|_w = \frac{P_x}{\rho \nu}. \tag{A3}$$

Here,  $P_x = dP/dx$ .

Second, substituting (A2) and (A3) into (A1), we have

$$U^+ = y^+ + \frac{P_x \nu}{2\rho \tau_w^{3/2}} y^{+2} + O(y^{+3}), \tag{A4}$$

where  $U^+ = U/u_\tau(t)$ ,  $y^+ = u_\tau(t)y/\nu$ ,  $u_\tau(t) = \sqrt{\tau_w(t)/\rho}$ , and  $\nu$  is the kinematic viscosity. The second term is subjected to the effect of pressure gradients. This explains the deviation of the mean flow from the canonical linear scaling in the viscous sublayer.

For an equilibrium channel,  $P_x \delta / (2\rho \tau_w Re_\tau) = -0.5/Re_\tau$ , and the second term in the Taylor expansion is  $-0.001y^{+2}$ , which amounts to  $-0.025$  at  $y^+ = 5$ . For a boundary layer

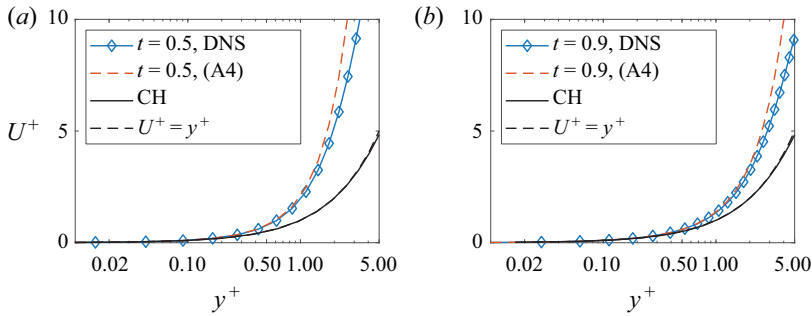


Figure 11. The mean velocity profile in the viscous sublayer of (a) R5A100 and (b) R10A100. The markers show the grid point locations.

subjected to a strong APG, e.g. case R5A100,  $P_x \delta / (2\rho\tau_w Re_\tau) = 50/Re_\tau \approx 0.1$ , and the second term in the Taylor expansion is  $0.1y^{+2}$ , which amounts to 2.5 at  $y^+ = 5$ .

Figure 11 shows the mean velocity profiles in the viscous sublayer. The profiles are normalized via the wall stress, viscosity and fluid density. For brevity, we present results in the two cases with the strongest APGs. The time instants are such that the effects of the imposed APGs have already manifested. We have the following two observations. First, the mean velocity profiles follow the linear scaling up to about  $y^+ \approx 0.4$  and  $0.7$  in figures 11(a,b), respectively, and this region contains 6 and 9 grid points in, respectively. Second, the quadratic scaling (A4) is a more powerful scaling than the linear scaling.

#### REFERENCES

- ANDERSON, J. 2011 *Fundamentals of Aerodynamics*. McGraw Hill.
- AUBERTINE, C.D. & EATON, J.K. 2005 Turbulence development in a non-equilibrium turbulent boundary layer with mild adverse pressure gradient. *J. Fluid Mech.* **532**, 345–364.
- BOBKE, A., VINUESA, R., ÖRLÜ, R. & SCHLATTER, P. 2017 History effects and near equilibrium in adverse-pressure-gradient turbulent boundary layers. *J. Fluid Mech.* **820**, 667–692.
- CHUNG, Y.M. 2005 Unsteady turbulent flow with sudden pressure gradient changes. *Intl J. Numer. Meth. Fluids* **47** (8–9), 925–930.
- COLEMAN, G.N., GARBARUK, A. & SPALART, P.R. 2015 Direct numerical simulation, theories and modelling of wall turbulence with a range of pressure gradients. *Flow Turbul. Combust.* **95**, 261–276.
- COLEMAN, G.N. & SPALART, P.R. 2015 Direct numerical simulation of turbulent Couette–Poiseuille flow with zero skin friction. In *European Turbulence Conference 2015*. Delft, The Netherlands.
- DING, L., SAXTON-FOX, T., HULTMARK, M. & SMITS, A.J. 2019 Effects of pressure gradients and streamline curvature on the statistics of a turbulent pipe flow. In *11th International Symposium on Turbulence and Shear Flow Phenomena*. TSFP 2019.
- GALBRAITH, R.A.M.D., SJOLANDER, S. & HEAD, M.R. 1977 Mixing length in the wall region of turbulent boundary layers. *Aeronaut. Q.* **28**, 97–110.
- GRAHAM, J., et al. 2016 A web services accessible database of turbulent channel flow and its use for testing a new integral wall model for LES. *J. Turbul.* **17**, 181–215.
- GRIFFIN, K.P., FU, L. & MOIN, P. 2021 Velocity transformation for compressible wall-bounded turbulent flows with and without heat transfer. *Proc. Natl Acad. Sci. USA* **118**, e2111144118.
- HARUN, Z., MONTY, J.P., MATHIS, R. & MARUSIC, I. 2013 Pressure gradient effects on the large-scale structure of turbulent boundary layers. *J. Fluid Mech.* **715**, 477–498.
- HE, S. & SEDDIGHI, M. 2015 Transition of transient channel flow after a change in Reynolds number. *J. Fluid Mech.* **764**, 395–427.
- HUANG, P.G. & COLEMAN, G.N. 1994 Van Driest transformation and compressible wall-bounded flows. *AIAA J.* **32**, 2110–2113.
- INOUE, M., PULLIN, D.I., HARUN, Z. & MARUSIC, I. 2013 LES of the adverse-pressure gradient turbulent boundary layer. *Intl J. Heat Fluid Flow* **44**, 293–300.

- JOHNSTONE, R., COLEMAN, G.N. & SPALART, P.R. 2010 The resilience of the logarithmic law to pressure gradients: evidence from direct numerical simulation. *J. Fluid Mech.* **643**, 163–175.
- KAWAI, S. & LARSSON, J. 2012 Wall-modeling in large eddy simulation: length scales, grid resolution, and accuracy. *Phys. Fluids* **24**, 015105.
- KIM, J., MOIN, P. & MOSER, R. 1987 Turbulence statistics in fully developed channel flow at low Reynolds number. *J. Fluid Mech.* **177**, 133–166.
- KITSIOS, V., SEKIMOTO, A., ATKINSON, C., SILLERO, J.A., BORRELL, G., GUNGOR, A.G., JIMÉNEZ, J. & SORIA, J. 2017 Direct numerical simulation of a self-similar adverse pressure gradient turbulent boundary layer at the verge of separation. *J. Fluid Mech.* **829**, 392–419.
- KNOPP, T., REUTHER, N., NOVARA, M., SCHANZ, D., SCHÜLEIN, E., SCHRÖDER, A. & KÄHLER, C.J. 2021 Experimental analysis of the log law at adverse pressure gradient. *J. Fluid Mech.* **918**, A17.
- LEE, J.H. 2017 Large-scale motions in turbulent boundary layers subjected to adverse pressure gradients. *J. Fluid Mech.* **810**, 323–361.
- LEE, J.-H. & SUNG, H.J. 2009 Structures in turbulent boundary layers subjected to adverse pressure gradients. *J. Fluid Mech.* **639**, 101–131.
- LEE, M. & MOSER, R.D. 2015 Direct numerical simulation of turbulent channel flow up to  $Re_\tau \approx 5200$ . *J. Fluid Mech.* **774**, 395–415.
- LOZANO-DURÁN, A., GIOMETTO, M.G., PARK, G.I. & MOIN, P. 2020 Non-equilibrium three-dimensional boundary layers at moderate Reynolds numbers. *J. Fluid Mech.* **883**, A20.
- LOZANO-DURÁN, A. & JIMÉNEZ, J. 2014 Effect of the computational domain on direct simulations of turbulent channels up to  $Re_\tau = 4200$ . *Phys. Fluids* **26**, 011702.
- MARUSIC, I., MONTY, J.P., HULTMARK, M. & SMITS, A.J. 2013 On the logarithmic region in wall turbulence. *J. Fluid Mech.* **716**, R3.
- MATHUR, A., GORJI, S., HE, S., SEDDIGHI, M., VARDY, A.E., O'DONOGHUE, T. & POKRAJAC, D. 2018 Temporal acceleration of a turbulent channel flow. *J. Fluid Mech.* **835**, 471–490.
- MELLOR, G.L. & GIBSON, D.M. 1966 Equilibrium turbulent boundary layers. *J. Fluid Mech.* **24**, 225–253.
- MODESTI, D. & PIROZZOLI, S. 2019 Direct numerical simulation of supersonic pipe flow at moderate Reynolds number. *Intl J. Heat Fluid Flow* **76**, 100–112.
- MODESTI, D., PIROZZOLI, S. & GRASSO, F. 2019 Direct numerical simulation of developed compressible flow in square ducts. *Intl J. Heat Fluid Flow* **76**, 130–140.
- MONTY, J.P., HARUN, Z. & MARUSIC, I. 2011 A parametric study of adverse pressure gradient turbulent boundary layers. *Intl J. Heat Fluid Flow* **32**, 575–585.
- MONTY, J.P., HUTCHINS, N., NG, H.C.H., MARUSIC, I. & CHONG, M.S. 2009 A comparison of turbulent pipe, channel and boundary layer flows. *J. Fluid Mech.* **632**, 431–442.
- MORRILL-WINTER, C., PHILIP, J. & KLEWICKI, J. 2017 An invariant representation of mean inertia: theoretical basis for a log law in turbulent boundary layers. *J. Fluid Mech.* **813**, 594–617.
- NAGIB, H.M. & CHAUHAN, K.A. 2008 Variations of von Kármán coefficient in canonical flows. *Phys. Fluids* **20** (10), 101518.
- NICKELS, T.B. 2004 Inner scaling for wall-bounded flows subject to large pressure gradients. *J. Fluid Mech.* **521**, 217–239.
- PARTHASARATHY, A. & SAXTON-FOX, T. 2022 A novel experimental facility to impose unsteady pressure gradients on turbulent boundary layers. *Exp. Fluids* **63** (6), 1–14.
- PERRY, A.E. 1966 Turbulent boundary layers in decreasing adverse pressure gradients. *J. Fluid Mech.* **26**, 481–506.
- PERRY, A.E., BELL, J.B. & JOUBERT, P.N. 1966 Velocity and temperature profiles in adverse pressure gradient turbulent boundary layers. *J. Fluid Mech.* **25** (2), 299–320.
- PERRY, A.E., MARUSIC, I. & JONES, M.B. 1998 New evolution equations for turbulent boundary layers in arbitrary pressure gradients. *Sadhana* **23** (5), 443–457.
- PERRY, A.E., MARUSIC, I. & JONES, M.B. 2002 On the streamwise evolution of turbulent boundary layers in arbitrary pressure gradients. *J. Fluid Mech.* **461**, 61–91.
- PERRY, A.E. & SCHOFIELD, W.H. 1973 Mean velocity and shear stress distributions in turbulent boundary layers. *Phys. Fluids* **16** (12), 2068–2074.
- ROMERO, S.K., ZIMMERMAN, S.J., PHILIP, J. & KLEWICKI, J.C. 2022a Stress equation based scaling framework for adverse pressure gradient turbulent boundary layers. *Intl J. Heat Fluid Flow* **93**, 108885.
- ROMERO, S., ZIMMERMAN, S., PHILIP, J., WHITE, C. & KLEWICKI, J. 2022b Properties of the inertial sublayer in adverse pressure-gradient turbulent boundary layers. *J. Fluid Mech.* **937**, A30.
- SCHLATTER, P. & ÖRLÜ, R. 2010 Assessment of direct numerical simulation data of turbulent boundary layers. *J. Fluid Mech.* **659**, 116–126.

- SMITS, A.J., MCKEON, B.J. & MARUSIC, I. 2011 High-Reynolds number wall turbulence. *Annu. Rev. Fluid Mech.* **43**, 353–375.
- SPALART, P.R. & WATMUFF, J.H. 1993 Experimental and numerical study of a turbulent boundary layer with pressure gradients. *J. Fluid Mech.* **249**, 337–371.
- STRATFORD, B.S. 1959 The prediction of separation of the turbulent boundary layer. *J. Fluid Mech.* **5** (1), 1–16.
- SUBRAHMANYAM, M., XU, Z., CANTWELL, B. & ALONSO, J.J. 2023 A new wall-stress model for large-eddy simulations. In *AIAA SCITECH 2023 Forum*, p. 0285. AIAA ARC.
- SUBRAHMANYAM, M.A., CANTWELL, B.J. & ALONSO, J.J. 2022 A universal velocity profile for turbulent wall flows including adverse pressure gradient boundary layers. *J. Fluid Mech.* **933**, A16.
- TOWNSEND, A.A. 1956 The properties of equilibrium boundary layers. *J. Fluid Mech.* **1**, 561–573.
- TRETTEL, A. & LARSSON, J. 2016 Mean velocity scaling for compressible wall turbulence with heat transfer. *Phys. Fluids* **28**, 026102.
- VAN DRIEST, E.R. 1951 Turbulent boundary layer in compressible fluids. *J. Aeronaut. Sci.* **18** (3), 145–160.
- VAN DRIEST, E.R. 1956 On turbulent flow near a wall. *J. Aeronaut. Sci.* **23** (11), 1007–1011.
- VOLINO, R.J. 2020 Non-equilibrium development in turbulent boundary layers with changing pressure gradients. *J. Fluid Mech.* **897**, A2.
- VOLPIANI, P.S., IYER, P.S., PIROZZOLI, S. & LARSSON, J. 2020 Data-driven compressibility transformation for turbulent wall layers. *Phys. Rev. Fluids* **5** (5), 052602.
- WEI, T., FIFE, P. & KLEWICKI, J. 2007 On scaling the mean momentum balance and its solutions in turbulent Couette–Poiseuille flow. *J. Fluid Mech.* **573**, 371–398.
- WEI, T., MACIEL, Y. & KLEWICKI, J. 2017 Integral analysis of boundary layer flows with pressure gradient. *Phys. Rev. Fluids* **2** (9), 092601.
- YANG, X.I.A., HONG, J., LEE, M. & HUANG, X.L.D. 2021 Grid resolution requirement for resolving rare and high intensity wall-shear stress events in direct numerical simulations. *Phys. Rev. Fluids* **6**, 054603.
- YANG, X.I.A. & LV, Y. 2018 A semi-locally scaled eddy viscosity formulation for LES wall models and flows at high speeds. *Theor. Comput. Fluid Dyn.* **32**, 617–627.